Molecular BioSystems

Accepted Manuscript

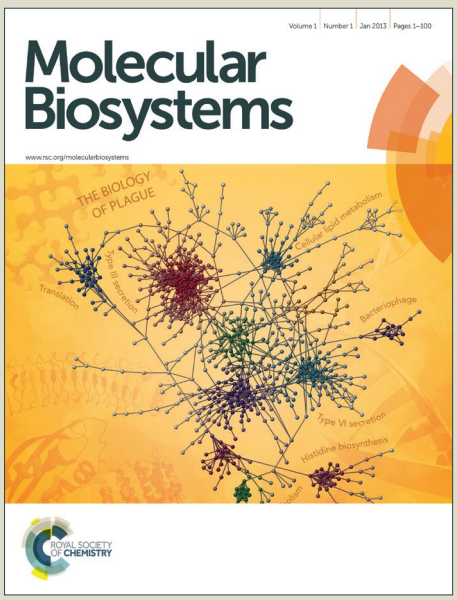

ROYAL SOCIETY OF CHEMISTRY

www.rsc.org/molecularbiosystems

Journal Name

RSCPublishing

ARTICLE

Exploring the mode of action of dithranol therapy for psoriasis: a metabolomic analysis using HaCaT cells.

Cite this: DOI: 10.1039/x0xx00000x

Katherine A. Hollywood [1 2], Catherine L. Winder [1 4], Warwick B. Dunn [5], Yun Xu [1 3], David Broadhurst [6], Christopher E.M. Griffiths [7] & Royston Goodacre [1 3]

Received 00th January 2012,
Accepted 00th January 2012

DOI: 10.1039/x0xx00000x

www.rsc.org/

Psoriasis is a common, immune-mediated inflammatory skin disease characterized by red, heavily scaled plaques. The disease affects over one million people in the UK and causes significant physical, psychological and societal impact. There is limited understanding regarding the exact pathogenesis of the disease although it is believed to be a consequence of genetic predisposition and environmental triggers. Treatments vary from topical therapies, such as dithranol, for disease of limited extent (< 5% body surface area) to the new immune-targeted biologic therapies for severe psoriasis. Dithranol (also known as anthralin) is a topical therapy for psoriasis believed to work by inhibiting keratinocyte proliferation. To date there have been no metabolomics-based investigations into psoriasis. The HaCaT cell line is a model system for the epidermal keratinocyte proliferation characteristic of psoriasis and was thus chosen for study. Dithranol was applied at therapeutically relevant doses to HaCaT cells. Following the optimisation of enzyme inactivation and metabolite extraction, gas chromatography-mass spectrometry was employed for metabolomics as this addresses central metabolism. Cells were challenged with 0-0.5 µg/mL in 0.1 µg/mL steps and this quantitative perturbation generated data that were highly amenable to correlation analysis. Thus, we used a combination of traditional principal components analysis, hierarchical cluster analysis, along with correlation networks. All methods highlighted distinct metabolite groups, which had different metabolite trajectories with respect to drug concentration and the interpretation of these data established that cellular metabolism had been altered significantly and provided further clarification of the proposed mechanism of action of the drug.

1. Manchester Institute of Biotechnology (MIB), University of Manchester, 131 Princess Street, Manchester, M1 7DN, UK.
2. Faculty of Life Science, University of Manchester, Manchester, M13 9PT, UK.
3. School of Chemistry, University of Manchester, Manchester, M1 7DN, UK.
4. School of Chemical Engineering and Analytical Science, University of Manchester, Manchester, M1 7DN, UK.
5. School of Biosciences, University of Birmingham, Edgbaston, Birmingham, B15 2TT, UK.
6. Department of Medicine, University of Alberta, Edmonton, Alberta, T6G 2EI, Canada.
7. The Dermatology Centre, Salford Royal NHS Foundation Trust, University of Manchester, Manchester Academic, Health Science Centre, Manchester, M6 8HD, U.K.

To whom correspondence should be addressed: Royston Goodacre, Manchester Institute of Biotechnology (MIB), University of Manchester, 131 Princess Street, Manchester, M1 7DN, UK, Tel.: (+44) 0161 306 4480; E-mail: Roy.Goodacre@manchester.ac.uk

INTRODUCTION

Psoriasis is a chronic immune-mediated inflammatory skin disease that affects approximately 2-3% of the world population. The disease manifests as red, heavily scaled plaques most commonly on the scalp, elbows or knees although any skin surface can be affected. Nail involvement and inflammatory arthritis may occur in up to 50% and 30% of patients respectively. Psoriasis is currently incurable and can produce significant psychosocial disability for those it afflicts resulting in high rates of depression. Most cases present before the age of 35 years and the disease is usually life-long. Plaques are characterised by epidermal keratinocyte proliferation and loss of differentiation accompanied by an inflammatory infiltrate. Underlying pathomechanisms are beginning to be understood and it is known to be a genetically predisposed condition that is triggered and exacerbated by environmental factors including streptococcal infection. Management of psoriasis is dictated for the most part by extent, in that limited

disease (< 5% body surface area affected) is treated with topical therapies including vitamin D3, corticosteroids and dithranol. An understanding of immune mechanisms involved in psoriasis has transformed the management of severe psoriasis with the advent of new biologic therapies targeted at cytokines including tumour necrosis factor alpha and interleukins 23 and 17.

Dithranol, one of the oldest yet most effective of topical therapies is known to accumulate in the cellular mitochondria [1]. However due to drug interactions being host specific (that is to say these may be different between different individuals as is any drug toxicity) [2] and the unpredictable nature of psoriasis incidence and flare, cell-based analyses are still popular in the area of psoriasis; therefore, in this study we used HaCaT cells [3]. These are an immortalised keratinocyte cell line, that display a keratin expression pattern typical of that seen in psoriatic epidermis and are thus invaluable cellular skin models. These cells were dosed with various levels of dithranol that caused a minimal amount of apoptosis [4-6].
Metabolomics is an analytical science, which aims to measure low molecular weight molecules present in cells, tissues or organisms that are involved in metabolic processes [7,8] and is becoming an increasingly popular science aimed at understanding biochemical processes. An important factor in any metabolomic-based analysis on a cellular system is the effective quenching of that system and this depends on whether the cells are in suspension [9,10] or adherent [11,12]. HaCaT cells are adherent, attach to the bottom of the culture flask and can readily be separated from culture supernatant. Moreover, unlike other adherent cells (*e.g.* Hela) they are not contact inhibited and thus grow as a layer; hence are very good mimics for skin making them a highly relevant model for psoriasis. After quenching cellular metabolism, metabolites are extracted [13-16] and analysed by a variety of analytical techniques [17] so as to maximise the coverage of the metabolome.

In order to probe the response of HaCaT cells to various doses of dithranol we used profiling metabolomics using gas chromatography-mass spectrometry (GC-MS). The metabolites one would expect to detect with this technique are those involved in central carbon and amino acid metabolism. We used GC-MS following protocols initially pioneered by Fiehn and colleagues [18], and refined by Dunn and co-workers [19,20]. These incorporated in-house metabolite standards so that most metabolites are identified definitively and ensuring we were wholly compliant with the Metabolomics Standards Initiative (MSI) [21].

A dose-response approach was used to investigate the response of the HaCaT cells to dithranol. To interrogate the resulting metabolomic dose-response data it is typical to use multivariate discriminant statistical models such as partial least squares-discriminant analysis, Fisher's linear discriminant analysis (also referred to as discriminant function analysis or canonical variate analysis); however, due to the dose-response nature of these data, resorting to such methods was theoretically inappropriate, and ultimately unnecessary (Partial least squares-regression (PLS-R) was however performed as a comparative analysis and for completeness of the manuscript results from which are shown in SI). Instead, for this study on a whole, we employed classical univariate hypothesis testing, together with three complementary multivariate correlation based methodologies. These included the rather traditional exploratory analyses of principal components analysis (PCA) [22] and hierarchical cluster analysis (HCA) [23,24] as well as a more novel correlation network approach [25,26]. Although similar in theoretical basis, each method helped build up a clear picture of metabolite perturbation in a unique manner.

EXPERIMENTAL PROCEDURES

Cell Culture and Drug Exposure

Drug compounds and reagents were purchased from Sigma Aldrich (Gillingham, UK), and cell culture consumables from GIBCO (Invitrogen Group, Paisley UK), unless otherwise stated.

All culture work was conducted within a Microflow biological safety cabinet and all work areas thoroughly cleaned with 70% ethanol before use. The cell culture medium utilised in this work was Dulbecco's Modified Eagle Medium (DMEM) supplemented with 10% Foetal Bovine Serum (FBS) and to avoid any bias in this undefined reagent we used a single batch. All DMEM used in this work also originated from a single batch. 1% Penicillin (5000 units/mL) and Streptomycin (50 mg/mL) were used to inhibit bacterial and fungal growth. To ensure

sufficient biomass for GC-MS analysis HaCaT cell growth was conducted in 225 cm^2 culture flasks utilising standard cell culture procedures.

Dithranol was applied when cells were determined by microscopy to be ~90% confluent and then incubated further for 24 h. Dithranol was dissolved in 100% acetone and applied to the cells to give a final concentration range of 0.1-0.5 µg/mL (0.4-2.2 µM) in 0.1 µg/mL steps. In addition to these 5 concentrations a control was used which involved the application of acetone only at the relevant volume. All drug solutions were made afresh before application to the cells. As shown in Figure 1 all drug exposures plus control were performed in triplicate. Microscopic inspection was undertaken and no obvious differences in cell confluency or cell structure were observed between the control and drug treated flasks after 24 h and the concentration range of dithranol was comparable with doses that induce minimal apoptosis in highly confluent HaCaT cells [4-6].

Metabolome Sample Preparation

Sample preparation was performed as detailed in Figure 1. Briefly both the cells as well as the spent culture media (footprint or exometabolome) [27] were analysed. The method for cellular analysis was essentially the same as Teng *et al.* [28], but rather than washing with ice cold phosphate buffered saline (PBS) we used room temperature PBS (15 mL) in order to reduce temperature shock to the cells. This brief washing (Fig. 1; step 6) took *ca*. 5 s, after which the cells were quenched and extracted using 100% methanol (7 mL, -48 °C) and detached from the surface by scraping the cells with a disposable cell scraper (Corning, UK). The methanol/cell mixture was then transferred to a centrifuge tube for extraction. Extraction was aided by three freeze-thaw cycles to liberate as many metabolites as possible [9]. After centrifugation (14°C, 5 min, 16200 *g*) to pellet the cell debris the supernatant was stored at -80°C.

The spent culture media were aspirated from each culture flask and filtered through a 0.45 µm pore size cellulose acetate membrane syringe filter to remove any remaining cellular debris. The filtered metabolic footprint samples were aliquoted (1 mL) into centrifuge tubes and immediately snap frozen in liquid nitrogen. All samples were stored at -80°C.

Metabolome GC-MS Analysis

Footprint (200 µL) and fingerprint (1 mL) aliquots (7 mL in total) were spiked with 100 µL internal standard solution (1.32 mg/mL succinic d_4 acid, 1.12 mg/mL malonic d_2 acid, 1.08 mg/mL glycine d_5); vortex mixed and lyophilised overnight (Eppendorf Vacufuge Concentrator 5301, Eppendorf, UK).

A two-stage chemical derivatisation was performed on the dried sample, 80 µL of 20 mg/mL O-methylhydroxylamine solution was added and heated at 40°C for 90 min followed by addition of 80 µL MSTFA (N-acetyl-N-[trimethylsilyl]-trifluoroacetamide) and heating at 40°C for 90 min. 20 µL of a retention index solution (4 mg/mL n-decane, n-dodecane, n-pentadecane, n-nonadecane, n-docosane dissolved in hexane) was added and the samples were analysed in a random order using a Agilent 6890 N gas chromatograph and 7683 autosampler (Agilent Technologies, Stockport, UK) coupled to a LECO Pegasus III electron impact time-of-flight mass spectrometer (LECO Corporation, St Joseph, USA) as detailed in [20,29]. Initial data processing of raw data was undertaken using LECO ChromaTof v2.12 software to construct a data matrix (metabolite peak *vs*. sample no.) including response ratios (peak area metabolite/peak area succinic-d_4 acid internal standard) for each metabolite peak in each sample.

Metabolite identifications were assigned through searching and matching against an in-house constructed library and also the NIST02 and Golm metabolome libraries. A definitive match (MSI level 1) means that the retention index and mass spectrum match that of an authentic standard analysed on the same instrument [30]. A putative match (MSI level 2) implies that the mass spectrum can be matched only to a non-Manchester library and cannot be confirmed *via* an in-house comparison. This process corresponds with the minimum reporting standards proposed for chemical analysis detailed within [21].

Data Analysis

Profiled data were separated into two data matrices (fingerprint, footprint). Each matrix had the dimensions 18 samples (3 biological replicates for each dosage concentration of 0-0.5 μg/mL (0-2.2 μM) in 0.1 μg/mL steps) by the number of reproducibly detected (< 20% missing values) metabolite features (this resulted in 127 metabolite features). The data were row normalized using probabilistic quotient normalization (PQN) [31] to equalize signal intensities to a reference profile, *i.e.* to reduce any variance arising from subtly differing dilutions of the biological extracts. Missing values were replaced by the lowest measured value for the given metabolite divided by two – as an approximation of a value below the limit of detection. Data were $\log_2$ transformed, both to stabilize variance, and in order to approximate a multivariate normal distribution for each treatment group. Unidentified metabolites were then removed from both data sets and subsequently disqualified from further data analysis.

For each remaining metabolite in turn, the null hypothesis that there are no differences in population means between the dosage groups was tested using one-way ANOVA. Correction for multiple comparisons was performed using the method described by Benjamini and Hochberg [32] and corrected *p*-values were reported. Principal components analysis (PCA) was then performed [33]. PCA is routinely used in metabolomics studies to visualize the principal multivariate variance in high-dimensional metabolomic data *via* mathematical projection into (usually) a two- or three-dimensional orthogonal subspace (principal components; PCs). A scatter plot of *PC score* vectors (a "scores plot"), where each point represents an individual sample, can be used to identify biologically interpretable patterns and/or clusters. When a specific PC score is related to a phenotype of interest, such as time course or group information, the corresponding *PC loading* vector (a mathematical vector describing of the influence of each metabolite feature on the PC score) is evaluated to discern biological inferences [22]. Bootstrap resampling/remodelling was used to determine which metabolites contributed significantly to the PCA loadings vector following standard protocol for multivariate models [34,23].

Unsupervised two-way agglomerative hierarchical cluster analysis (HCA) then assessed the similarities between individual metabolomic profiles [23,35]. This algorithm used a multivariate Euclidean distance metric and Ward's group linkage. The results were displayed as a heat map (green=low metabolite concentration, red=high metabolite concentration) with associated cluster dendrograms; the lower the linkage distances in the dendrogram the more similar the feature. Metabolites that were most similar across all samples, and samples that were most similar across all metabolites, form the lowest linkage in the respective dendrograms; thus emergent clusters will have similar characteristics. Prior to PCA and HCA each metabolite feature was scaled to unit variance (autoscaled), which allows each metabolite to be compared within the analysis with no bias due to differences in absolute concentration variance [24,36].

Finally, the strength and direction of the linear relationship between all identified metabolite features was determined by calculating pairwise Pearson's correlation coefficient (*r*). The results of the resulting correlation matrix were presented in the form of a spring-embedded correlation plot [26]. Here a network of "nodes" and "spring-edges" are constructed such that each node represents each of the tested metabolite features and the spring constant of each edge is proportional to the correlation coefficient between two connected nodes. The size of each node is proportional to significance of that variable; the larger the node the lower the *p*-value. Edges were only included in the network if the correlation coefficient was positive, and significant at a critical *p*-value of < 0.05. Once the network is constructed it is allowed to "relax". That is to say, the connected spring-edges compete against each other to "pull" the nodes in a given direction based on the spring constant (the higher the correlation, the stiffer the spring, and hence the more power organizing the clustering of the node). Once relaxed (*i.e.* the model is in a low energy configuration) the spring embedded plot can be viewed as a simple multivariate cluster analysis, where nodes that cluster close to each other can be considered to be highly correlated in a multivariate sense. Node colour directly maps onto the Pearson's correlation between metabolite concentration and drug concentration (Red = positive correlation; Blue = negative correlation); nodes were coloured "grey" in the plot if their corresponding *p*-value was > 0.05. Networks were constructed using the graph visualization software – Graphviz (www.graphviz .org) using the '*neato'* virtual physics model [37].

All of the statistical analyses were performed using the Matlab® scripting language, version R2014a (http://www.mathworks.com).

RESULTS

The analysis of dithranol treated HaCaT cells yielded 127 metabolite features from the intra-cellular metabolome (fingerprint), of which 47 were uniquely identified to level 1 of the MSI (*i.e.* defined to a standard and on the same instrument), and 107 metabolite features for the metabolic footprint, of which 40 were uniquely identified. One-way ANOVA was used to determine the changes in each metabolite in both the footprint and fingerprint data testing the null hypothesis that there are no differences in population means between the dosage groups.

For the footprint data, after correction for multiple comparisons, none of the 40 identified metabolites were significant (using a critical adjusted p-value of < 0.05 and a false discovery rate of 5%) – data not shown.

For the fingerprint data, after correcting for multiple comparisons, 32 of the 47 identified metabolites were significant (see Table 1). This suggests that whilst there is a large effect on cellular metabolism, very little signal is excreted into the culture media and thus perhaps also indicates that cellular integrity has not been compromised. That is to say, the cells have not died and leaked metabolites into the culture media; this is largely because the experiment was designed to be below lethal levels of drug (see above). Table 1 also lists the identified metabolites according to MSI [21]. Additional information is also provided to include the associated human metabolome database (HMBD) accession number, the chemical formulae and the primary pathways associated with the identified metabolite.

The results of PCA (Figure 2) illustrates no significant clustering or correlations between drug concentration of the footprint data (Figure 2a), bootstrap resampling showed that no metabolites significantly contributed to this model – data not shown. Conversely, the PCA of the fingerprint data (Figure 2b) shows clear clustering, whereby PC1 describes a linear negative correlation with drug concentration, and PC2 describes clear separation of concentration group '0.3' from the others. Bootstrap resampling revealed that 22 metabolites were uniquely significant contributors to PC1, 9 metabolites were uniquely significant contributors to PC2, and 8 metabolites were significantly contributing in both PC1 and PC2 (see Table 1 and Figure 3).

HCA clarifies the complex inter-relationship between metabolite and drug concentration found in the fingerprint data (see Figure 4). The "sample" dendrogram (x-axis) reflects exactly the clustering presented in the PCA scores plot (Figure 2b). However, the "metabolite" dendrogram (y-axis) reveals 3 clear metabolite clusters (labelled A, B and C). Within clusters A and B there are sub-clusters (A1, A2, A3, B1, and B2). These clusters are labelled in, and provide the structure for, Table 1. Each of these 6 clusters demonstrates a general concentration trajectory with respect to drug concentration. For example, the metabolites in cluster C rapidly change from high metabolite concentration to low metabolite concentration at around 0.2 µg/mL; whereas, Cluster B2 rapidly changes from low to high at 0.2 µg/mL and then back to low at 0.5 µg/mL. Figure 5 a-f shows representative metabolites from each of these sub-cluster trajectories. HCA for the footprint data confirmed the PCA results and showed no clear clustering – data not shown. The spring-embedded correlation plots for the fingerprint data corroborated the HCA results (see Figure 6). In this instance we have included the unidentified metabolites (labelled KH_x) to illustrate their compliance with the general structure presented for the identified metabolites in the main text. There is clearly a large cluster of significant metabolites (red) that match up with cluster C in the HCA. Additionally there is a cluster of significant metabolites (dark blue) that match up with clusters A3 and B1. Finally there is a cluster (light blue / green /yellow) which match with cluster B2. HCA clusters A1 maps to the linkage between the main clusters at the top of the spring plot, and cluster A2 maps to the linkage between the main clusters at the bottom of the spring plot but were not univariately significant and are therefore coloured "grey". These results reflect the univariate statistics presented in Table 1. As there were no univariately significant metabolites in the footprint data no corresponding spring-embedded correlation plot was generated.

DISCUSSION

A large number of metabolites were not only significantly altered in cells exposed to dithranol but were also correlated in different ways to the dithranol level *i.e*. correlation groups A1-3, B1-2 & C1. It would be unrealistic to attempt to interpret individual box and whisker plots for each metabolite without the inclusion of additional biochemical information. It was for this reason that a metabolic map was manually constructed utilising information gained from within the KEGG database (Figure 7). The relevant pathways highlighted in the study are summarised in Figure 7. These include glycolysis, TCA cycle, amino acid metabolism and the urea cycle. The reconstructed biochemical map is further restricted to include only the measured metabolites (shown in black text, for ease of visualization) and therefore there are 'gaps' in this pathway reconstruction. For example, glycolysis only comprises glucose, glucose-6-phosphate and pyruvate and not all the intermediate steps, as these were not detected in the samples. These metabolites do of course exist in our in-house database but are absent because they are found below the limit of detection. A limited number of metabolites that were not identified in the samples are shown (depicted in red) to highlight important reference points. The metabolites present in the DMEM culture media are shown in orange to highlight if any of the observed changes are associated with nutrient depletion. A box and whisker plot is included to show relative metabolite levels as the drug exposure increases from 0-0.5 µg/mL.

From this metabolite analysis it is possible to begin to understand and interpret the role of these metabolites that vary and are co-correlated upon drug exposure. It is clearly evident from Figure 2 and 5 that dithranol has a pronounced affect on the metabolism of HaCaT cells. It is necessary to combine *a priori* literature-based information with the current results to develop an understanding of the mode of action of dithranol for psoriasis treatment. The most important features are briefly discussed below.

A number of metabolites exhibited a decreasing linear response with increased dithranol concentration. These included malonate, nicontinamide, glycerol-3-phosphate, myo-inositol and hypotaurine. These downstream metabolites have varying roles and are likely indicators of decreased cellular metabolism.

Mitochondrial response

The exact mode of action of dithranol therapy for psoriasis is not fully understood. Possible theories of the mode of action suggest that the activity of glucose-6-phosphatase is inhibited by dithranol [38] or the most documented theory is that dithranol accumulates or has inhibitory effects in the mitochondria. Thus inhibiting mitochondrial oxidative respiration and thereby restricting ATP synthesis [1,38].

Our findings support the hypothesis that dithranol inhibits the TCA cycle in that we observed a decrease in the two TCA intermediates that were measured (*viz*. citrate and malate) belonging to correlation Group C1 (decrease with respect to increasing dithranol dose). We also observed changes in the metabolite levels of intermediates involved in glycolysis. At the higher concentrations of dithranol (0.3-0.5 µg/mL) accumulation of glucose, glucose-6-phosphate, pyruvate and lactate was observed. The accumulation of glycolytic intermediates indicates an impaired flux through the TCA cycle, thereby supporting the proposed mode of action of dithranol in the TCA cycle. Our findings do not support the theory that glucose-6-phosphatase is inhibited by dithranol as we observe a positive correlation in the concentration of glucose and glucose-6-phosphate. This is primarily due to dithranol being applied in our study at a much lower concentration to previous investigations (~44 µM *vs.* 2.2 µM) [38] and therefore unlikely to cause cell death or apoptosis (as detailed elsewhere). The response relationship discussed above for all these metabolites indicates that dithranol has a clear effect on central metabolism of the HaCaT cells. This indicates that the drug has successfully penetrated the cells, and does indeed seem to be targeting the mitochondria.

Amino acid response

The re-constructed metabolite map clearly highlights that cellular amino acid concentrations are affected by dithranol exposure. The degree of the effect differs from amino acid to amino acid. The most linear response to dithranol concentration is observed for glutamate, aspartate (Group C1) and histidine (Group B1). Glutamate is shown to decrease almost linearly with increased dithranol treatment, which follows the trend observed by the TCA

intermediates. Aspartate shows a similar decrease in concentration as the concentration of dithranol increases to almost depleted levels at 0.4 & 0.5 μg/mL. Conversely, the concentration of histidine increases with the increasing concentration of dithranol.

The remaining amino acids exhibit variable responses upon dithranol treatment. Glycine (Group A1) is at its highest level in the control cells and shows minimal correlation to dithranol concentration. Tryptophan (Group A2) greatly increases in concentration at 0.1 μg/mL before decreasing at 0.2 μg/mL and gradually rising again as the concentration of dithranol increases. Leucine (Group A3) shows a gradual increase in concentration as the concentration of dithranol increases and is almost linear in its response at the highest concentrations of drug. The amino acids serine, tyrosine and valine were classified within correlation group B1. These metabolites exhibit an almost positive parabolic response to increasing levels of drug, with the largest increase occurring between 0.2 and 0.3 μg/mL. Group B2, contains the amino acids alanine, isoleucine, methionine, phenylalanine & threonine. These amino acids increase in concentration from control to a maximum at 0.3 μg/mL exposure before reducing in concentration again at 0.4 & 0.5 μg/mL dithranol treatment.

The question arises as to why this variable response may be occurring? We know from our own experimental work and the literature [5,6,4] that HaCaT cells are still viable thus making apoptosis or cell death unlikely in the case of amino acid depletion. We also acknowledge that to support the growth of the HaCaT cells the DMEM culture media is rich in the majority of these afore-mentioned amino acids and so the transport of the amino acids into the cell may be complicating the observed metabolic response. Although the variable response observed in the amino acid profiles is not fully understood with further targeted investigation of the amino acids is may provide useful information to elucidate further knowledge of the specific mode of action of dithranol.

CONCLUSION

Many of the metabolites detected by GC-MS analysis were significantly affected by dithranol treatment. HCA classified these significantly affected metabolites into 6 response groups. These collections of metabolites followed different trajectories with respect to increasing levels of dithranol and thus may reflect common effects on metabolism. Of course this is not guaranteed as correlation does not equate to effect [39] thus endorsing the importance of biochemical interpretations. Biological interpretation of our results has highlighted two areas of metabolism whose response to dithranol treatment is of interest, namely mitochondrial and amino acid metabolism. The effect on mitochondrial and NAD(P)H has been previously reported in other HaCaT cellular studies [1] and in patients undergoing therapy with dithranol which supports our theory that metabolomics is a very powerful approach to investigate the mode of action of drugs. By contrast, there has been very little reported on the reduction of amino acid levels by increasing concentrations of dithranol suggesting that these important protein synthesis building blocks are required elsewhere in the cell. Our findings indicate that the changes observed in the amino acid profiles are not related purely to the effect of the drug on cellular metabolism. Thus, it appears that targeted analysis of the amino acids will shed further light onto the mechanism of action of dithranol therapy.

ACKNOWLEDGEMENTS

K.A.H. and R.G. thank Stiefel Laboratories (U.K.) Ltd. for funding and R.G. is also very grateful to UK BBSRC for funding.

REFERENCES

1. McGill A, Frank A, Emmett N, Turnbull DM, Birch-Machin MA, Reynolds NJ (2005) The anti-psoriatic drug anthralin accumulates in keratinocyte mitochondria, dissipates mitochondrial membrane potential, and induces apoptosis through a pathway dependent on respiratory competent mitochondria. FASEB journal : official publication of the Federation of American Societies for Experimental Biology 19 (8):1012-1014. doi:10.1096/fj.04-2664fje
2. Goodacre R (2007) Metabolomics of a superorganism. Journal of Nutrition 137 (1):259S-266S
3. Boukamp P, Petrussevska RT, Breitkreutz D, Hornung J, Markham A, Fusenig NE (1988) NORMAL KERATINIZATION IN A SPONTANEOUSLY IMMORTALIZED ANEUPLOID HUMAN KERATINOCYTE CELL-LINE. Journal of Cell Biology 106 (3):761-771. doi:10.1083/jcb.106.3.761
4. Klem EB (1978) EFFECTS OF ANTI-PSORIASIS DRUGS AND METABOLIC-INHIBITORS ON GROWTH OF EPIDERMAL-CELLS IN CULTURE. Journal of Investigative Dermatology 70 (1):27-32. doi:10.1111/1523-1747.ep12543421
5. George SE, Anderson RJ, Haswell M, Groundwater PW (2013) An investigation of the effects of dithranol-induced apoptosis in a human keratinocyte cell line. Journal of Pharmacy and Pharmacology 65 (4):552-560. doi:10.1111/jphp.12019
6. Henseleit U, Rosenbach T, Kolde G (1996) Induction of apoptosis in human HaCaT keratinocytes. Arch Dermatol Res 288 (11):676-683. doi:Doi 10.1007/Bf02505277
7. Hollywood K, Brison DR, Goodacre R (2006) Metabolomics: current technologies and future trends. Proteomics 6 (17):4716-4723. doi:10.1002/pmic.200600106
8. Dunn WB, Broadhurst DI, Atherton HJ, Goodacre R, Griffin JL (2011) Systems level studies of mammalian metabolomes: the roles of mass spectrometry and nuclear magnetic resonance spectroscopy. Chemical Society reviews 40 (1):387-426. doi:10.1039/b906712b
9. Winder CL, Dunn WB, Schuler S, Broadhurst D, Jarvis R, Stephens GM, Goodacre R (2008) Global metabolic profiling of Escherichia coli cultures: an evaluation of methods for quenching and extraction of intracellular metabolites. Analytical chemistry 80 (8):2939-2948. doi:10.1021/ac7023409
10. Sellick CA, Hansen R, Maqsood AR, Dunn WB, Stephens GM, Goodacre R, Dickson AJ (2009) Effective quenching processes for physiologically valid metabolite profiling of suspension cultured Mammalian cells. Analytical chemistry 81 (1):174-183. doi:10.1021/ac8016899
11. Dettmer K, Nurnberger N, Kaspar H, Gruber MA, Almstetter MF, Oefner PJ (2011) Metabolite extraction from adherently growing mammalian cells for metabolomics studies: optimization of harvesting and extraction protocols. Analytical and Bioanalytical Chemistry 399 (3):1127-1139. doi:10.1007/s00216-010-4425-x
12. Lorenz MA, Burant CF, Kennedy RT (2011) Reducing Time and Increasing Sensitivity in Sample Preparation for Adherent Mammalian Cell Metabolomics. Analytical chemistry 83 (9):3406-3414. doi:10.1021/ac103313x
13. Hutschenreuther A, Kiontke A, Birkenmeier G, Birkemeyer C (2012) Comparison of extraction conditions and normalization approaches for cellular metabolomics of adherent growing cells with GC-MS. Analytical Methods 4 (7):1953-1963. doi:10.1039/c2ay25046b
14. Bi HC, Krausz KW, Manna SK, Li F, Johnson CH, Gonzalez FJ (2013) Optimization of harvesting, extraction, and analytical protocols for UPLC-ESI-MS-based metabolomic analysis of adherent mammalian cancer cells. Analytical and Bioanalytical Chemistry 405 (15):5279-5289. doi:10.1007/s00216-013-6927-9
15. Sellick CA, Hansen R, Stephens GM, Goodacre R, Dickson AJ (2011) Metabolite extraction from suspension-cultured mammalian cells for global metabolite profiling. Nature protocols 6 (8):1241-1249. doi:10.1038/nprot.2011.366
16. Dietmair S, Timmins NE, Gray PP, Nielsen LK, Kromer JO (2010) Towards quantitative metabolomics of mammalian cells: Development of a metabolite extraction protocol. Analytical Biochemistry 404 (2):155-164. doi:10.1016/j.ab.2010.04.031
17. Dunn WB, Broadhurst DI, Atherton HJ, Goodacre R, Griffin JL (2011) Systems level studies of mammalian metabolomes: the roles of mass spectrometry and nuclear magnetic resonance spectroscopy. Chemical Society reviews 40 (1):387-426. doi:10.1039/b906712b
18. Fiehn O, Kopka J, Dormann P, Altmann T, Trethewey RN, Willmitzer L (2000) Metabolite profiling for plant functional genomics. Nature biotechnology 18 (11):1157-1161. doi:10.1038/81137
19. Begley P, Francis-McIntyre S, Dunn WB, Broadhurst DI, Halsall A, Tseng A, Knowles J, Goodacre R, Kell DB (2009) Development and performance of a gas chromatography-time-of-flight mass spectrometry

analysis for large-scale nontargeted metabolomic studies of human serum. Analytical chemistry 81 (16):7038-7046. doi:10.1021/ac9011599
20. Dunn WB, Broadhurst D, Begley P, Zelena E, Francis-McIntyre S, Anderson N, Brown M, Knowles JD, Halsall A, Haselden JN, Nicholls AW, Wilson ID, Kell DB, Goodacre R (2011) Procedures for large-scale metabolic profiling of serum and plasma using gas chromatography and liquid chromatography coupled to mass spectrometry. Nature protocols 6 (7):1060-1083. doi:10.1038/nprot.2011.335
21. Sumner LW, Amberg A, Barrett D, Beale MH, Beger R, Daykin CA, Fan TWM, Fiehn O, Goodacre R, Griffin JL, Hankemeier T, Hardy N, Harnly J, Higashi R, Kopka J, Lane AN, Lindon JC, Marriott P, Nicholls AW, Reily MD, Thaden JJ, Viant MR (2007) Proposed minimum reporting standards for chemical analysis. Metabolomics 3 (3):211-221. doi:10.1007/s11306-007-0082-2
22. Ringner M (2008) What is principal component analysis? Nature biotechnology 26 (3):303-304. doi:Doi 10.1038/Nbt0308-303
23. Hastie T.; Tibshirani R FJ (2009) The Elements of Statistical Learning: Data Mining, Interference, and Prediction. 2nd edn. Springer, New York
24. van den Berg RA, Hoefsloot HCJ, Westerhuis JA, Smilde AK, van der Werf MJ (2006) Centering, scaling, and transformations: improving the biological information content of metabolomics data. Bmc Genomics 7. doi:Artn 142
Doi 10.1186/1471-2164-7-142
25. Ebbels TM, Buxton BF, Jones DT (2006) springScape: visualisation of microarray and contextual bioinformatic data using spring embedding and an 'information landscape'. Bioinformatics (Oxford, England) 22 (14):e99-107. doi:10.1093/bioinformatics/btl205
26. Broadhurst DI, Kell DB (2006) Statistical strategies for avoiding false discoveries in metabolomics and related experiments. Metabolomics 2 (4):171-196. doi:Doi 10.1007/S11306-006-0037-Z
27. Kell DB, Brown M, Davey HM, Dunn WB, Spasic I, Oliver SG (2005) Metabolic footprinting and systems biology: The medium is the message. Nature Reviews Microbiology 3 (7):557-565. doi:10.1038/nrmicrol177
28. Teng Q, Huang WL, Collette TW, Ekman DR, Tan C (2009) A direct cell quenching method for cell-culture based metabolomics. Metabolomics 5 (2):199-208. doi:10.1007/s11306-008-0137-z
29. O'Hagan S, Dunn WB, Brown M, Knowles JD, Kell DB (2005) Closed-loop, multiobjective optimization of analytical instrumentation: Gas chromatography/time-of-flight mass spectrometry of the metabolomes of human serum and of yeast fermentations. Analytical chemistry 77 (1):290-303. doi:10.1021/ac049146x
30. Brown M, Dunn WB, Dobson P, Patel Y, Winder CL, Francis-McIntyre S, Begley P, Carroll K, Broadhurst D, Tseng A, Swainston N, Spasic I, Goodacre R, Kell DB (2009) Mass spectrometry tools and metabolite-specific databases for molecular identification in metabolomics. Analyst 134 (7):1322-1332. doi:10.1039/b901179j
31. Dieterle F, Ross A, Schlotterbeck G, Senn H (2006) Probabilistic quotient normalization as robust method to account for dilution of complex biological mixtures. Application in H-1 NMR metabonomics. Analytical chemistry 78 (13):4281-4290. doi:Doi 10.1021/Ac051632c
32. Benjamini Y, Hochberg Y (1995) Controlling the False Discovery Rate - a Practical and Powerful Approach to Multiple Testing. J Roy Stat Soc B Met 57 (1):289-300
33. Jolliffe I, T. (2002) Principal Component Analysis. 2nd Edition edn. Springer-Verlag, New York
34. Peres-Neto PR, Jackson DA, Somers KM (2003) Giving meaningful interpretation to ordination axes: Assessing loading significance in principal component analysis. Ecology 84 (9):2347-2363. doi:Doi 10.1890/00-0634
35. Kaufman LR, P.J. (1990) Finding Groups in Data: An Introduction to Cluster Analysis. 1st edn. John Wiley, New York
36. Xia JG, Broadhurst DI, Wilson M, Wishart DS (2013) Translational biomarker discovery in clinical metabolomics: an introductory tutorial. Metabolomics 9 (2):280-299. doi:Doi 10.1007/S11306-012-0482-9
37. Ellson J, Ganser ER, Koutsofios E, North SC, Woodhull G (2004) Graph Drawing Software. In: Junger M, Mutzel P (eds) Graphviz and Dynagraph- Static and Dynamic Graph Drawing Tools. Springer-Verlag, Berlin/Heidelberg, pp 127-148
38. Mahrle G (1997) Dithranol. Clinics in Dermatology 15 (5):723-737
39. Camacho D, de la Fuente A, Mendes P (2005) The origin of correlations in metabolomics data. Metabolomics 1 (1):53-63. doi:10.1007/s11306-005-1107-3

FIGURE LEGENDS

Figure 1: *A summary diagram to illustrate the successive stages in the collection of fingerprint and footprint samples.*

Figure 2: *PCA scores plots showing the variance across the concentration range of dithranol treatment for A) footprint and B) fingerprint samples.*

Figure 3: *PCA loadings illustrating the contribution of the metabolites towards PC1 or PC2. 22 metabolites were uniquely significant contributors to PC1, 9 metabolites were uniquely significant contributors to PC2, and 8 metabolites were significantly contributing in both PC1 and PC2.*

Figure 4: *Hierarchical Cluster Analysis (HCA) illustrating the complex inter-relationship between metabolite (y-axis RHS) and drug concentration (x-axis) found in the fingerprint data. Relative concentrations of metabolites are shown at high concentrations (Red) and low concentrations (Green). The response of the metabolites is then grouped according to response (y-axis, LHS).*

Figure 5: *Box and whisker plots of dithranol concentration (µg/mL) vs. relative metabolite concentration to illustrate the general trends observed from the correlation analysis for groups A1 (Glycine), A2 (Tryptophan), A3 (Leucine), and groups B1 (Serine), B2 (Threonine) and C1 (Pyroglutamate). Box and whisker plots provide a descriptive summary of the spread of replicate results.*

Figure 6: *Spring Embedded Correlation plot illustrating the metabolites (circles) and the associated correlations (lines/springs). The size of the circle is proportional to the significance of the metabolite (i.e. the larger the circle the more significant the metabolite) and the spring relates to the amount of correlation (the shorter the spring the more correlated the response of the metabolite to its neighbour).*

Figure 7: *Constructed metabolite map to illustrate the effect of dithranol treatment on HaCaT cells. The use of solid arrows indicates a direct linkage of metabolites while a dashed arrow corresponds to a pathway including a limited number of undetected metabolites. The metabolites in black are those which where successfully identified and those in red are included as a reference. Metabolites highlighted in orange are metabolites which are actively present in the DMEM culture media employed in the growth of the HaCaT cells. All box and whisker plots represent metabolites detected in the internal metabolome. Green features are provided for interest but are not metabolites.*

Table 1*: Identified metabolites from the internal metabolome of dithranol treated HaCaT cells. The table summarises in column i) the metabolite name, ii) the ANOVA F score, iii) p-value, iv & v) the response in PC 1 or PC2, vi) the HCA group, vii) HMDB assession number, viii) molecular formula, ix) primary pathway association & x) the MSI identification level.*

FIGURE 1

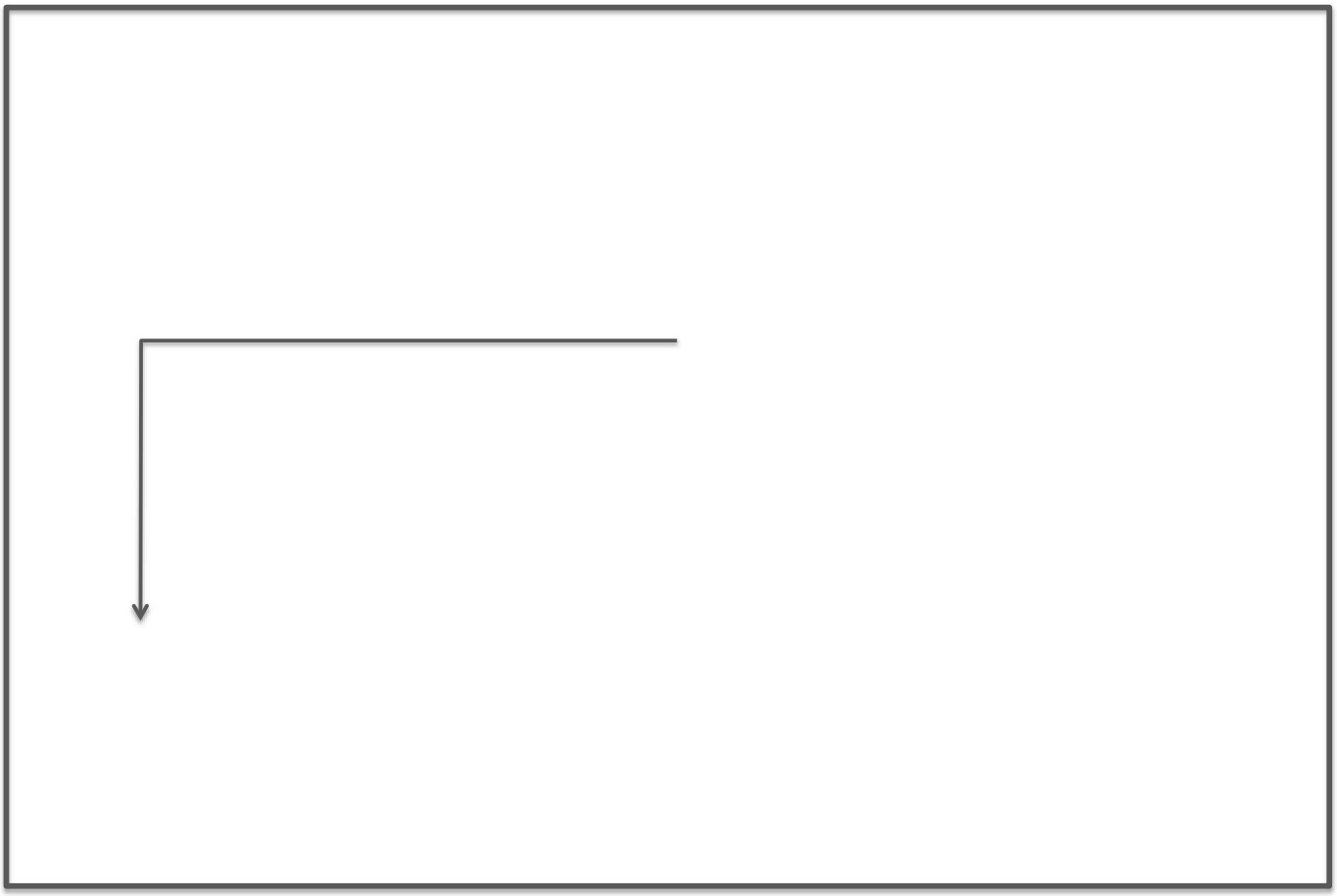

FIGURE 2

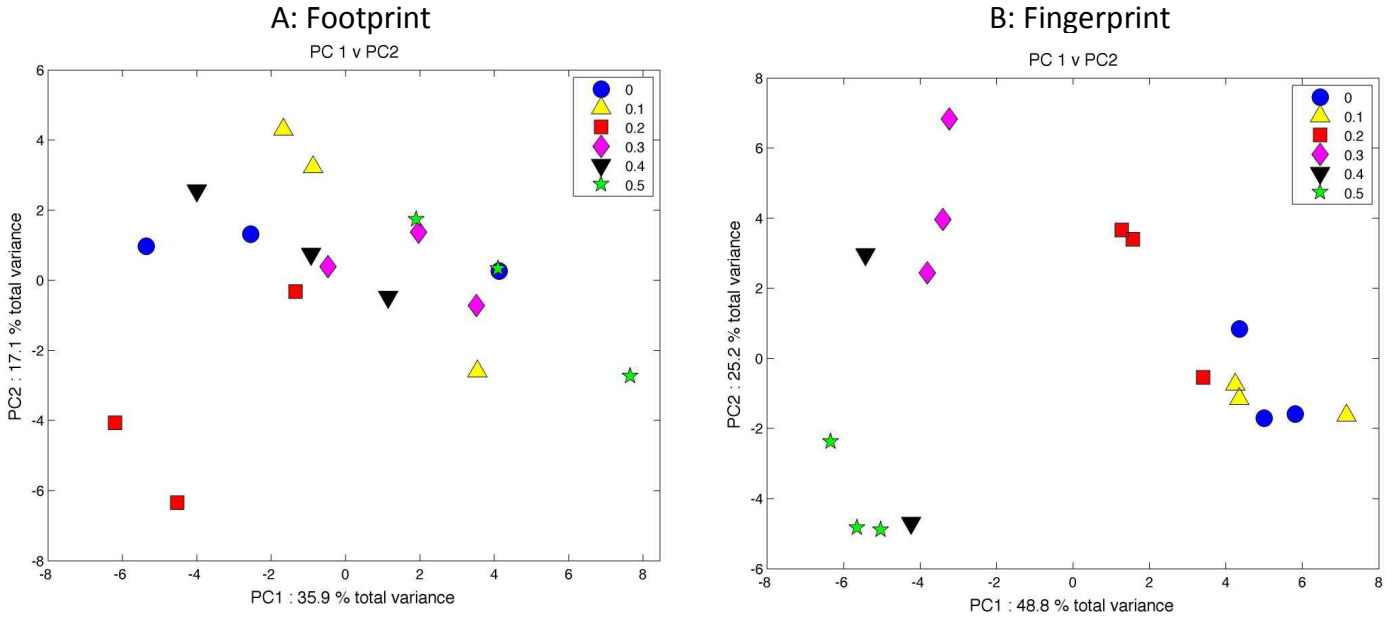

FIGURE 3

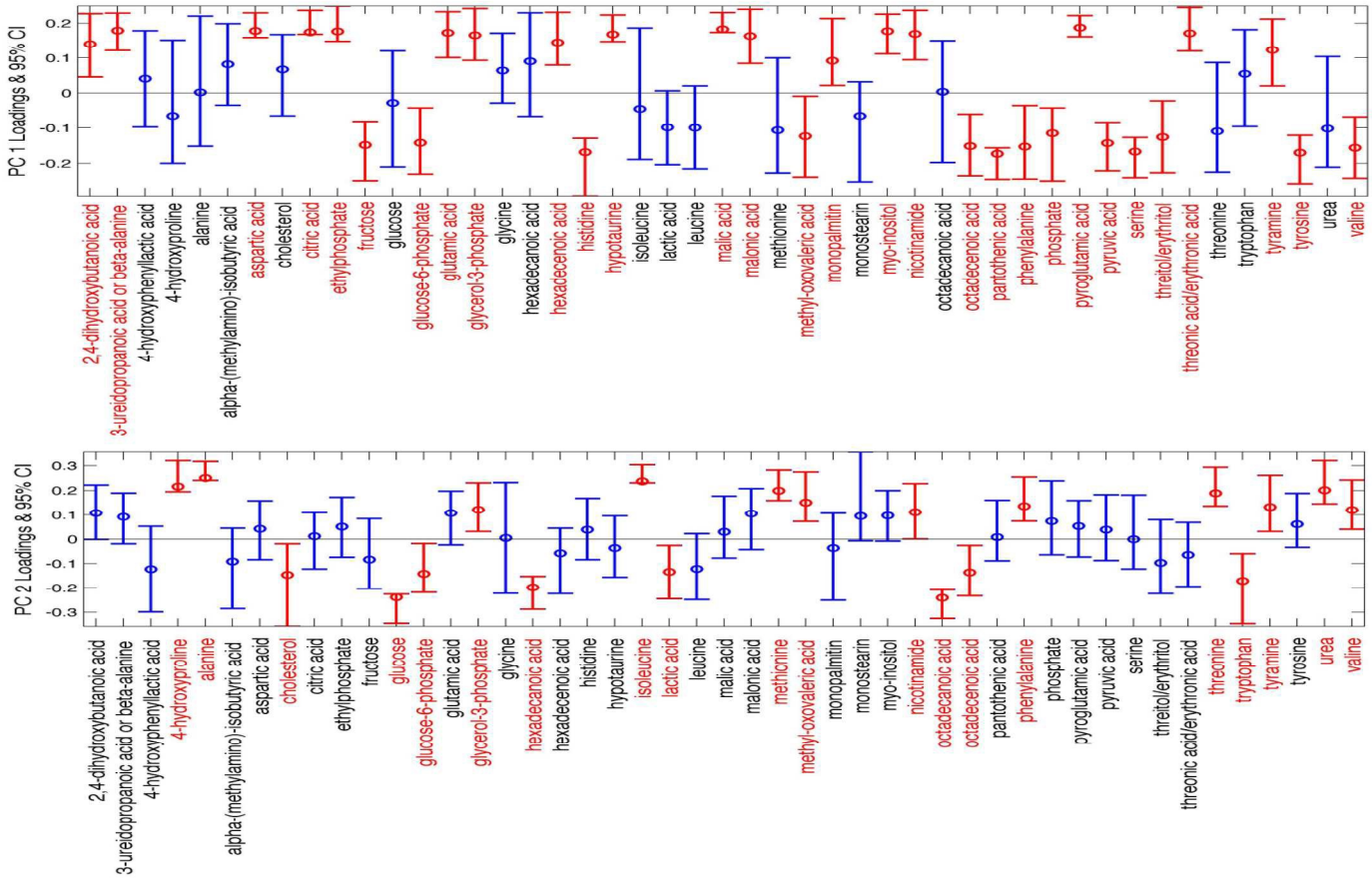

454 **FIGURE 4**

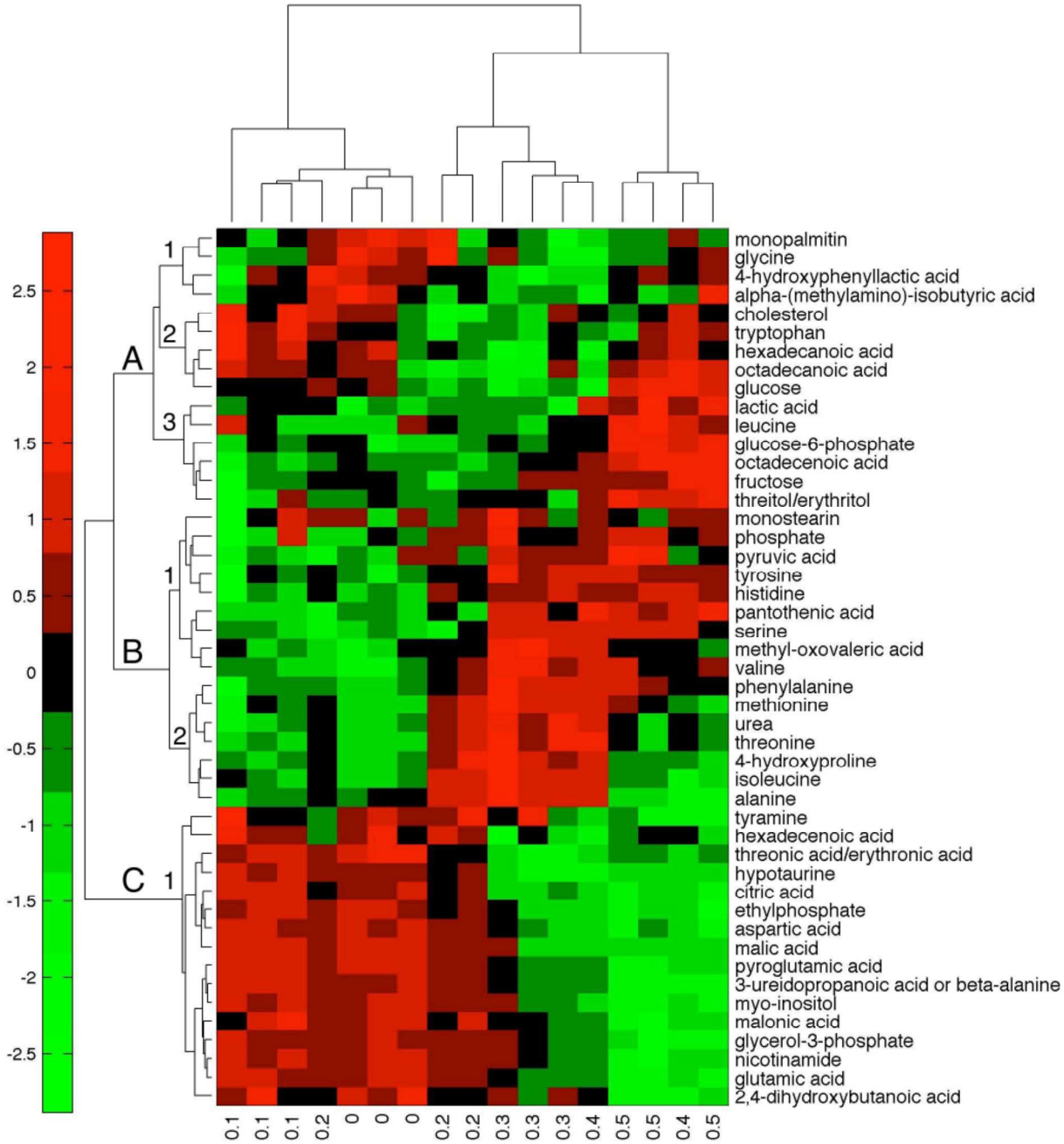

455
456

457 **FIGURE 5**
458

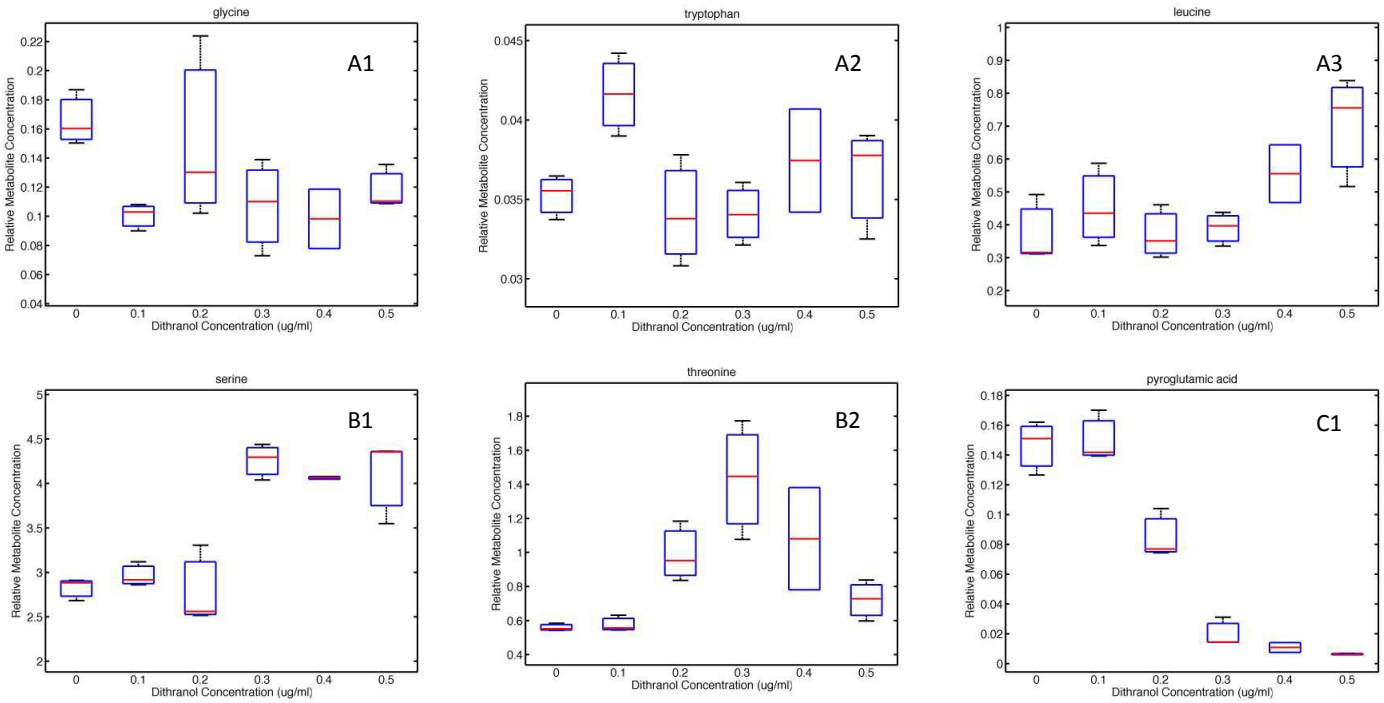

459
460
461

FIGURE 6

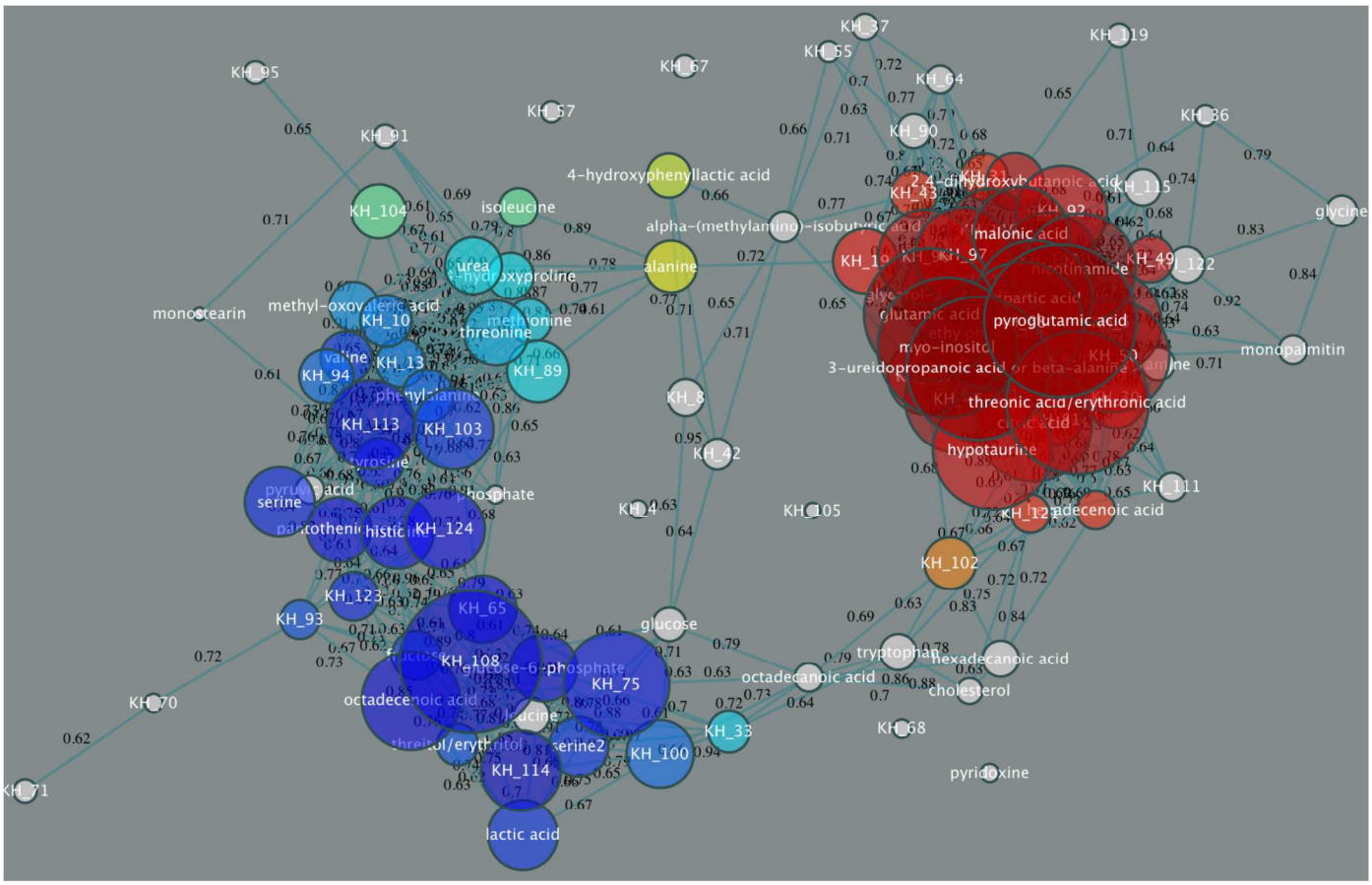

FIGURE 7

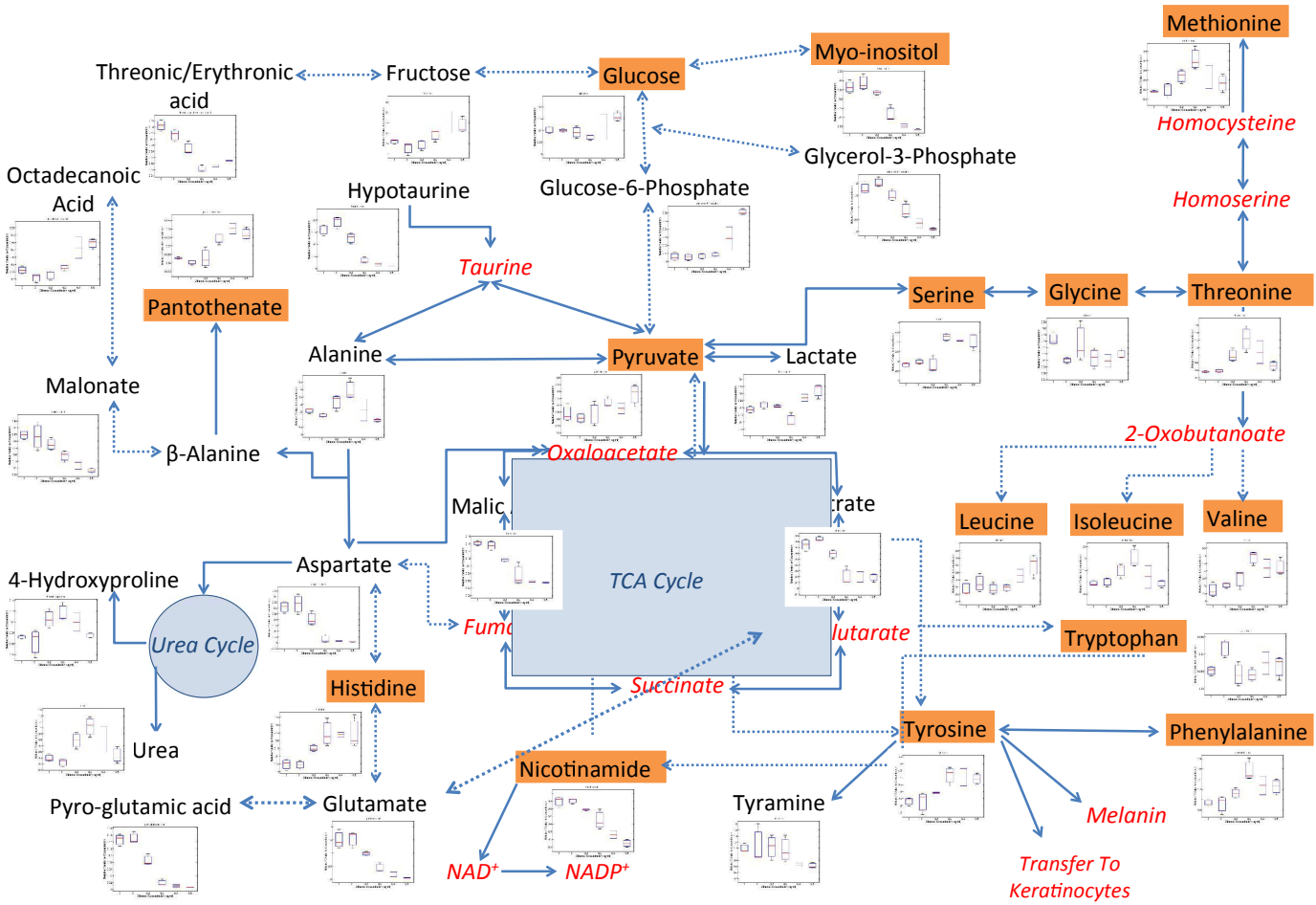

471 **TABLE 1**

Name	F(5,11)^	p-value*	PC1§	PC2§	HCA Group	HMDB Accession Number	Molecular Formula	Primary Pathways	MSI Identification Level
4-hydroxyphenyllactic acid	4.15	0.03			A1	HMDB00755	$C_9H_{10}O_4$	/	1
alpha-(methylamino)-isobutyric acid	2.19	0.15			A1	-	$C_5H_{11}NO_2$	/	1
glycine	2.10	0.15			A1	HMDB00123	$C_2H_5NO_2$	Amino Acid Metabolism	1
monopalmitin	2.10	0.15	+		A1	HMDB31074	$C_{19}H_{38}O_4$	/	1
cholesterol	1.49	0.28		-	A2	HMDB00067	$C_{27}H_{46}O$	/	1
glucose	2.65	0.10		--	A2	HMDB00122	$C_6H_{12}O_6$	Glycolysis, Pentose Phosphate & Galactose metabolism	1
hexadecanoic acid	2.74	0.10		--	A2	HMDB00220	$C_{16}H_{32}O_2$	/	1
octadecanoic acid	2.00	0.17		-	A2	HMDB00827	$C_{18}H_{36}O_2$	/	1
tryptophan	2.54	0.11		-	A2	HMDB00929	$C_{11}H_{12}N_2O_2$	Amino Acid Metabolism	1
fructose	4.75	0.02	--		A3	HMDB00660	$C_6H_{12}O_6$	Fructose and mannose metabolism & Galactose metabolism	1
glucose-6-phosphate	8.73	0.002	-	-	A3	HMDB01401	$C_6H_{13}O_9P$	Glycolysis & Pentose Phosphate	1
lactic acid	9.52	0.002	-	-	A3	HMDB01311	$C_3H_6O_3$	Glycolysis & pyruvate metabolism	1
leucine	3.51	0.06			A3	HMDB00687	$C_6H_{13}NO_2$	Amino Acid Metabolism	1
octadecenoic acid	14.88	0.0003	-	-	A3	HMDB00827	$C_{18}H_{36}O_2$	/	1
threitol/erythritol	3.30	0.07	-		A3	HMDB04136/HMDB02994	$C_4H_{10}O_4$	/	2
histidine	10.18	0.0021	--		B1	HMDB00177	$C_6H_9N_3O_2$	Amino Acid Metabolism	1
methyl-oxovaleric acid	6.39	0.009	-	+	B1	HMDB00491	$C_6H_{10}O_3$	Amino Acid Metabolism	1
monostearin	0.46	0.80			B1	HMDB31075	$C_{21}H_{42}O_4$	/	1
pantothenic acid	14.38	0.0006	--		B1	HMDB00210	$C_9H_{17}NO_5$	Beta-Alanine metabolism & Pantothenate and CoA biosynthesis	1
phosphate	1.18	0.39	-		B1	HMDB12228	$C_2H_7O_4P$	/	1
pyruvic acid	2.90	0.09	-		B1	HMDB00243	$C_3H_4O_3$	Glycolysis, TCA, Pentose Phosphate & amino acid metabolism	1
serine	15.00	0.0003	--		B1	HMDB03406	$C_3H_7NO_3$	Amino Acid Metabolism	1
tyrosine	5.35	0.02	--		B1	HMDB00158	$C_9H_{11}NO_3$	Amino Acid Metabolism	1
valine	6.34	0.009	-	+	B1	HMDB00883	$C_5H_{11}NO_2$	Amino Acid Metabolism	1
4-hydroxyproline	7.14	0.006		++	B2	HMDB00725	$C_5H_9NO_3$	Amino Acid Metabolism	1
alanine	6.23	0.010		++	B2	HMDB00161	$C_3H_7NO_2$	Amino Acid Metabolism	1
isoleucine	4.22	0.03		++	B2	HMDB00172	$C_6H_{13}NO_2$	Amino Acid Metabolism	1
methionine	4.57	0.03		++	B2	HMDB00696	$C_5H_{11}NO_2S$	Amino Acid Metabolism	1
phenylalanine	5.99	0.010	-	+	B2	HMDB00159	$C_9H_{11}NO_2$	Amino Acid Metabolism	1
threonine	10.09	0.0021		+	B2	HMDB00167	$C_4H_9NO_3$	Amino Acid Metabolism	1
urea	7.46	0.006		++	B2	HMDB00294	CH_4N_2O	Purine & Pyrimidine Biosythesis/Arginine & Proline Metabolism	1
2,4-dihydroxybutanoic acid	6.59	0.009	+		C1	HMDB00360	$C_4H_8O_4$	/	1
3-ureidopropanoic acid or beta-alanine	63.82	1.88E-06	++		C1	HMDB00026/HMDB00056	$C_4H_8N_2O_3/C_3H_7NO_2$	/	2
aspartic acid	31.34	2.21E-05	++		C1	HMDB06483	$C_4H_7NO_4$	Amino Acid Metabolism	1
citric acid	34.63	1.52E-05	++		C1	HMDB00094	$C_6H_8O_7$	TCA Cycle	1
ethylphosphate	26.29	4.27E-05	++		C1	HMDB12228	$C_2H_7O_4P$	/	1
glutamic acid	49.32	4.30E-06	++		C1	HMDB00094	$C_6H_8O_7$	TCA Cycle	1
glycerol-3-phosphate	19.42	1.57E-04	++	+	C1	HMDB00126	$C_3H_9O_6P$	Glycerolipid Metabolism/Glycerophosphlipid Metabolism	1
hexadecenoic acid	3.13	0.07	+		C1	/	$C_{16}H_{32}O_2$	Fatty Acid Metabolism	1
hypotaurine	35.10	1.52E-05	++		C1	HMDB00965	$C_2H_7NO_2S$	Taurine and Hypotaurine Metabolism	1
malic acid	21.69	1.00E-04	++		C1	HMDB00744	$C_4H_6O_5$	TCA Cycle, Pyruvate metabolism & Glyoxylate and Dicarboxylate Metabolism	1
malonic acid	18.46	1.84E-04	+		C1	HMDB00691	$C_3H_4O_4$	Pyrimidine metabolism/beta-Alanine metabolism	1
myo-inositol	61.05	1.88E-06	++		C1	HMDB00211	$C_6H_{12}O_6$	/	1
nicotinamide	29.28	2.77E-05	++		C1	HMDB01406	$C_6H_6N_2O$	Nicotinate and nicotinamide metabolism	1
pyroglutamic acid	83.36	1.08E-06	++		C1	HMDB00267/HMDB03339	$C_5H_7NO_3$	D-Glutamine and D-glutamate metabolism/Amino Acid Metabolism	2
threonic acid/erythronic acid	43.98	6.23E-06	+		C1	HMDB00943/HMDB00613	$C_4H_8O_5$	/	2
tyramine	2.84	0.09	+	+	C1	HMDB00306	$C_8H_{11}NO$	Tyrosine metabolism	1

§ +/- = significant positve/negative loading at p-value < 0.05; ++/-- = significant positve/negative loading at p-value < 0.005
* p-value adjusted for multiple comparsions using the Benjamini and Hochberg method using a false discovery rate of 0.05
^ ANOVA F-score with group d.f.= 5 and error d.f. = 11

472
473
474